Available online at www.sciencedirect.com
SCIENCE DIRECT®
International Journal of Heat and Mass Transfer 48 (2005) 3689–3706
International Journal of HEAT and MASS TRANSFER
www.elsevier.com/locate/ijhmt

Numerical investigation of a PCM-based heat sink with internal fins

V. Shatikian, G. Ziskind *, R. Letan

Heat Transfer Laboratory, Department of Mechanical Engineering, Pearlstone Center for Aeronautical Studies, Ben-Gurion University of the Negev, P.O. Box 653, Beer-Sheva 84105, Israel

Received 15 December 2003
Available online 2 June 2005

Abstract

The present study explores numerically the process of melting of a phase-change material (PCM) in a heat storage unit with internal fins open to air at its top. Heat is transferred to the unit through its horizontal base, to which vertical fins made of aluminum are attached. The phase-change material is stored between the fins. Its properties used in the simulations, including the melting temperature of 23–25 °C, latent and sensible specific heat, thermal conductivity and density in solid and liquid states, are based on a commercially available paraffin wax.

A detailed parametric investigation is performed for melting in a relatively small system, 5–10 mm high, where the fin thickness varies from 0.15 mm to 1.2 mm, and the thickness of the PCM layers between the fins varies from 0.5 mm to 4 mm. The ratio of the PCM layer to fin thickness is held constant. The temperature of the base varies from 6 °C to 24 °C above the mean melting temperature of the PCM.

Transient three- and two-dimensional simulations are performed using the Fluent 6.0 software, yielding temperature evolution in the fins and the PCM. The computational results show how the transient phase-change process, expressed in terms of the volume melt fraction of the PCM, depends on the thermal and geometrical parameters of the system, which relate to the temperature difference between the base and the mean melting temperature, and to the thickness and height of the fins.

In search for generalization, dimensional analysis of the results is performed and presented as the Nusselt numbers and melt fractions vs. the Fourier and Stefan numbers and fin parameters. In some cases, the effect of Rayleigh number is significant and demonstrated.

1. Introduction

Large heat-storage capacity of phase-change materials (PCMs) makes them attractive for use in various thermal energy storage systems where their latent heat is utilized. There exists a wide range of applications for such systems, from energy storage in buildings [1,2] to electronics cooling [3,4] and from material processing to thermal management of air- and spacecraft [5].

Theoretical and experimental studies in the field have yielded extensive literature on various aspects of the phase-change problems, including basic studies of phase-change phenomena, material properties,

* Corresponding author. Tel.: +972 8 6477089; fax: +972 8 6472813.
E-mail address: gziskind@bgu.ac.il (G. Ziskind).

0017-9310/$ - see front matter © 2005 Elsevier Ltd. All rights reserved.
doi:10.1016/j.ijheatmasstransfer.2004.10.042

Nomenclature

A_c	cross-section area (m^2)
C^*	fin efficiency parameter
c_p	specific heat at constant pressure (J/kg °C)
Fo	Fourier number, $\alpha t/(l_b/2)^2$; for fin $Fo_f = \alpha t/l_f^2$
$\hbar$	enthalpy (J/kg)
h	heat transfer coefficient (W/m^2 °C)
k	thermal conductivity (W/m °C)
l	length (m)
L	latent heat (J/kg)
Nu	Nusselt number, $(q''/\Delta T)((l_b/2)/k_{PCM})$
P	perimeter, m
q''	heat flux (W/m^2)
Ra	Rayleigh number, $g\beta\rho^2 c_p \Delta T l_f^3/(\mu k)$
Ste	Stefan number, $c_p\Delta T/L$
t	time (s)
T	temperature (°C or K)
u	velocity component (m/s)
V	volume (m^3)
x	Cartesian coordinate (m)

Greek symbols

α	volume fraction
β	volumetric expansion coefficient (1/K)
γ	liquid fraction
Δ	difference
η_f	fin efficiency
μ	dynamic viscosity (kg/m s)
ρ	density (kg/m^3)

Subscripts

b	PCM width
f	fin
i	component
ref	reference value
w	wall
PCM	phase-change material
t	fin width

mathematical modeling, numerical techniques, experimental methods, and heat transfer enhancement. As early as in 1971, Hale et al. [6] discussed the relationship between PCM and other thermal control techniques, provided detailed data on the material properties of "the most promising PCMs", and presented engineering considerations relevant to PCM systems design. Two other milestone publications on the subject are the book by Humphries and Griggs [7] and the fundamental work by Viskanta [8]. The former is a valuable source of property data and also presents a general parametric study of a model PCM system. The latter summarizes theoretical and numerical modeling of phase change and associated heat transfer in one- and multi-dimensional systems, and discusses the methods for heat transfer enhancement. More recently, an extensive review of physical phenomena associated with phase change in various geometries has been presented by Fukusaka and Yamada [9]. The latest review by Zalba et al. [10] deals with classification and properties of phase-change materials, heat transfer, and application of PCMs in energy storage. Both reviews reflect the significant progress made in the field during the last two decades, and contain above two hundred references each. There exists also a considerable body of literature dedicated to development and analysis of numerical techniques designated for phase-change processes. A review of mathematical modeling was presented by Hu and Argyropoulos [11], with special attention paid to the effects of convective motion in the liquid phase. Different physical models and numerical procedures were compared by Bertrand et al. [12] for a benchmark problem concerning a simulation of coupled natural convection and melting.

Following the classification given by Abhat [13] and Zalba et al. [10], the materials used for energy storage with solid–liquid phase change can be divided into organic and inorganic, like metals, alloys, and hydrated salts. Paraffins, which belong to the organic group, are suitable for heat storage applications as they have convenient melting temperatures, are non-toxic, recyclable, chemically inert, non-corrosive, and can withstand a large number of cycles.

The low thermal conductivity of paraffins presents, however, a significant challenge in design of heat storage systems. This is because during the phase change the solid–liquid interface always moves away from the boundary through which heat passes between the PCM and the surroundings: during solidification, a solid layer grows near a cooled surface, while in melting there is a growing liquid layer on the heated boundary. Since the only heat transfer mechanism through the solid layer is conduction, the heat transfer rate decreases when the thickness of this layer increases, and the low thermal conductivity of a PCM makes this thermal resistance too high for a required rate of phase change. In the liquid layer, the physical picture is much more complex, because natural convection can develop due to the temperature difference between the heated boundary and the solid part of the PCM. Existence of natural convection and its contribution to overall heat transfer depends on the geometry of the system and thickness of the liquid

layer; still, low thermal conductivity of the PCM inhibits the phase change.

In order to overcome this problem, various heat-transfer enhancement techniques have been suggested, like fins, metal and graphite-compound matrices, dispersed high-conductivity particles inside the PCM, and micro-encapsulation of PCM, as discussed by Velraj et al. [14] and Zalba et al. [10]. Design of PCM-based heat sinks for electronics has been analyzed by Pal and Joshi [15], who provide special recommendations concerning organic materials.

The use of fins was extensively discussed by Humphries and Griggs [7], for a PCM-filled cell of constant volume with a constant heat flux at one boundary. Pure conduction was assumed in the PCM, and its properties were assumed constant. Studies of PCM systems with extended surfaces were continued for various geometries, especially finned tubes (e.g. Ismail et al. [16]), where the numerical models were constructed neglecting density difference between the solid and liquid phases and assuming that there was no convection in the melt.

It was shown by Eftekhar et al. [17], however, that physical properties of paraffin waxes induced natural convection even in liquid layers of relatively small thickness. In their work, an experimental thermal storage system included two parallel plates, heated and cooled, separated by vertical fins. The storage cell was 53.5 mm high and 18.5 mm wide. The heated plate was located below the cooled plate so that the liquid layer eventually became unstable. This instability caused natural convection along the fins and at the solid–liquid interface, which, in turn, affected the rate of phase change.

The work by Eftekhar et al. [17] demonstrates that when a PCM-based heat storage system has conducting partitions, evolution of the melting front is influenced by both heat transfer from a primary heated surface and from a conducting partition, or fin, attached to it. In this connection, one can note that the problem of phase change in an enclosure with one heated surface has been studied extensively in the past, and the results of those studies are highly relevant also for the systems with internal fins, as discussed below.

Hale and Viskanta [18] performed an experimental and analytical study of melting and solidification of several PCMs, including *n*-octadecane, cooled or heated from above or below. It was found that when melting from below, the natural convection influences the heat transfer and the motion of the phase-change boundary during the process.

Ho and Viskanta [19] studied melting of *n*-octadecane from an isothermal vertical wall of a rectangular cavity 130 mm high, 50 mm wide, and 50 mm deep. In order to accommodate the volume expansion associated with the phase-change process from solid to liquid, a small air gap was maintained between the top of the material and the insulated top surface of the cavity. It has been shown that the time-wise variation of the molten volume fraction, V/V_0 could be expressed as a function of the Stefan number, *Ste*, the Fourier number, *Fo*, and the Rayleigh number, *Ra*.

Gadgil and Gobin [20] simulated numerically two-dimensional melting of a solid phase-change material in a rectangular enclosure heated from one side. Of special interest was the influence of the enclosure aspect ratio, *A*, on the melting curve, since this can be relevant to optimizing the dimensions of latent heat storage elements. The results of Gadgil and Gobin [20] show that *A* has a strong influence on the melting curve, e.g. an increase in *A* from 1.13 to 5.25 causing more than 16-fold decrease in the time required to melt 80% of the PCM.

The effect of free convection on the shape and motion of the melting front of gallium from a vertical wall was investigated by Gau and Viskanta [21], in a rectangular test cell which had inside dimensions of 8.89 cm in height, 6.35 cm in width, and 81 cm in depth. Their results reported clearly that for larger aspect ratio cavities, melting of the solid near the top may be greatly promoted, and melting near the base of the test cell may be completely terminated, due to free convection in the melt. At very early times, before the buoyancy-driven flow was initiated or when fluid motion was still very weak, the interface shape was flat and parallel to the heated wall of the test cell. Heat transfer was dominated by conduction. As the heating progressed, the buoyancy-driven convection in the melt started to develop and continued to intensify, yielding a non-uniform melt layer receding from the top to the bottom of the test cell.

Zhang and Bejan [22] have reported results of their study of the time-dependent melting within a relatively large enclosure 74 cm high (height/width ratio equals 5) filled with *n*-octadecane, subjected to a constant heat flux boundary condition. They show that for the heated plate itself, first its temperature rises from the ambient level to the melting point of the phase-change material. Then, there is a period when the temperature of the plate is uniform and rises linearly in time. Finally, the wall temperature reaches a plateau in the convection melting regime.

Pal and Joshi [23] studied computationally and experimentally melting of *n*-triacontane in a side heated tall enclosure of aspect ratio 10, by a uniformly dissipating heat source. They show how buoyancy driven convection in the molten PCM starts to develop. An implicit enthalpy-porosity approach was utilized for computational modeling of the melting process, and showed good agreement with the experiments.

In the problems of phase change in an enclosure with one heated surface, like those discussed above, longitudinal heat conduction in the enclosure boundaries is commonly neglected. The longitudinal conduction is,

however, important when conducting partitions are used, as shown by Eftekhar et al. [17] and most recently by Casano and Piva [24].

Lately, the details of heat transfer and phase change in the presence of cooling fins have become the focus of attention. Inaba et al. [25] presents a numerical study of solidification in a system in which rectangular tubes are arranged vertically in a heat storage vessel filled with a molten PCM, and plate fins are installed horizontally between those tubes. Their numerical results elucidate the flow pattern, velocity profile and heat transfer rate in the melted liquid layer, revealing that the amount of transported heat through the fins increased with the fin thickness, and the heat release completion time period was shortened. The completion time of heat release process decreased as the fin pitch decreased, due to the larger cooling area.

Lamberg and Siren [26] studied melting in a semi-infinite PCM storage cell with a thin horizontal fin of infinite length. The end-wall, which was at a constant temperature, and the fin act as heat transfer surfaces in the melting process. According to Lamberg and Siren [26], there are three stages in the melting process: pure conduction from the constant temperature end-wall and the fin, conduction from the fin with some natural convection from the end-wall, and finally only natural convection from the fin. An approximate analytical model has been proposed by Lamberg and Siren [27] for solidification in a system with two parallel heated walls and a horizontal fin of finite length which connects them.

The literature survey indicates that modeling of phase-change processes presents a significant challenge, due to complexity and conjunction of the involved physical phenomena. As mentioned above, various approaches are attempted to overcome these difficulties, commonly by neglecting one or more essential features of the process, e.g. volumetric expansion due to the phase change, convection in the liquid phase, and motion of the solid in the melt due to density differences. It has become common to use a two-dimensional model for three-dimensional situations [28], and to approximate certain terms in the conservation equations [29].

The present work is an attempt to overcome those limitations, and solve complete conservation equations simultaneously for solid fins, solid and liquid PCM, and air, while allowing for PCM expansion, convection in the fluid media (melted PCM and air), and solid phase motion in the liquid. This approach has been implemented successfully in the previous study by Shatikian et al. [30], where the processes of melting and solidification of a PCM have been studied numerically in one specific geometry, namely a partly enclosed space having vertical conducting plates attached to the base, which could be heated or cooled. Detailed temperature and phase fields have been obtained as functions of time, showing evolution of the heat transfer in the system as the phase-change material melts/solidifies. The change in the heat transfer rate with time, and the instantaneous temperature distributions inside the partitions and the PCM have been presented and discussed.

In the present work, the same approach is used for a detailed parametric investigation of melting in a relatively small system, having fins 5–10 mm high and 0.15–1.2 mm thick, with a PCM stored between the fins in layers 0.5–4 mm thick. The ratio of the PCM to fin thickness is held constant. The fins are attached to a constant temperature horizontal heated plate, the temperature of which varies from 6 °C to 24 °C above the mean melting temperature of the PCM.

In the following section, a physical model of the problem is introduced, and the numerical procedure is presented and discussed. Then, the time-dependent results for heat fluxes from the base and melt fractions of the PCM are presented in detail and discussed. Finally, an attempt is made to apply dimensional analysis in search for generalization of the results.

2. Numerical study

A physical model of the system is presented in detail below. Then, the computational procedure is discussed.

2.1. Physical model

A schematic view of the three-dimensional physical model is shown in Fig. 1a. Vertical plate-type fins are attached to a horizontal base which has a uniform temperature, T_w. Conducting end walls, identical to the fins, bound the system in the third direction. A phase change material fills the space above the base between the fins. As a result, heat is supplied to the PCM along all three coordinate axes. From above, the PCM is exposed to the ambient air. Thus, it is assumed that heat is transferred between the PCM and the base, the fins, the end walls and the ambient air. Heat transfer between the fin tips and the ambient is neglected.

The height of the fins and end walls is larger than the height of the solid PCM, which fills 85% of the space. This is done in order to accommodate a significant increase in the PCM volume during the solid–liquid phase transition, due to a large difference in solid and liquid density that exists in reality.

Geometrical dimensions explored in the present study are summarized in Table 1. The fins are made of aluminum, in order to ensure their high thermal conductivity. The properties of aluminum and air are summarized in Table 2. A density-temperature relation is used for air. In all the cases explored in this study, the model PCM was based on the properties of a commercially available paraffin wax (Rubitherm RT25), as discussed below.

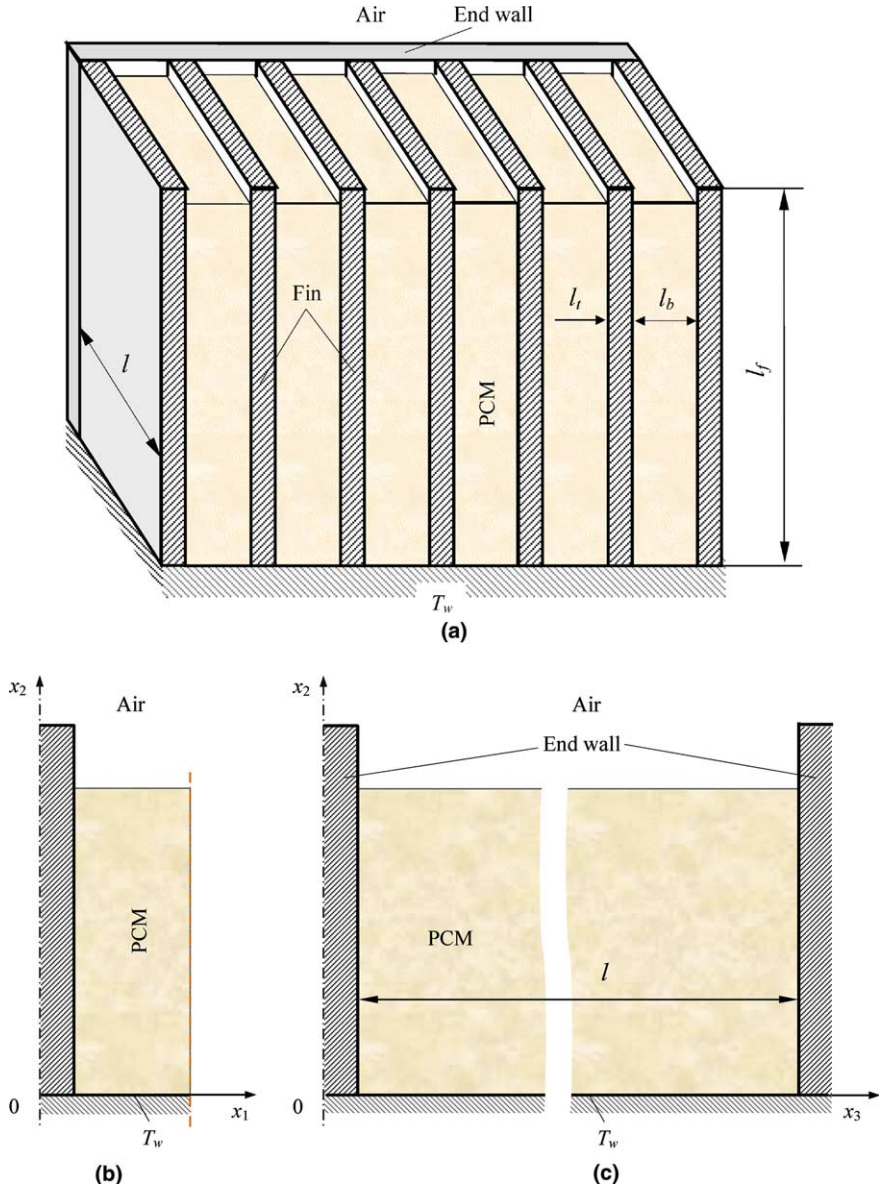

Fig. 1. Definition of the problem: (a) Three-dimensional physical model (front end wall is not shown); (b) computational domain, x_1–x_2 plane; and (c) computational domain, x_2–x_3 plane.

Table 1
Geometry parameters

Case	l_f, mm	l_t, mm	l_b, mm
1	10	1.2	4
2	10	0.6	2
3	10	0.3	1
4	10	0.15	0.5
5	5	0.6	2

For a detailed study of phase-change with internal fins, a relatively small system has been chosen, with the maximum fin length of 10mm. The overall width and length of the system would depend on its destination, but it is reasonable to assume that both dimensions are of few centimeters. Such system could serve, for example, as a basis for the development of a PCM-based heat sink for electronic equipment in a future study. The following parameter variations were chosen, as reflected in Table 1 (cases 1–5):

- the fin thickness varied from 0.15 mm to 1.2 mm;
- the PCM layer thickness between the fins varied from 0.5 mm to 4 mm;

Table 2
Properties of aluminum and air used for computation

Materials	Thermal conductivity (W/m K)	Density (kg/m^3)	Specific heat (J/kg K)
Aluminum	202.4	2719	871
Air	0.0242	$1.2\times10^{-5}T^2 - 0.01134T + 3.498$	1006.4

- the ratio of the fin thickness to the PCM layer thickness was kept constant, so that the amount of the PCM and aluminum in the sink were constant for a constant fin length, thus keeping its mass constant;
- in addition to the basic fin length of 10 mm, shorter fins of 5 mm have been explored. The amount (height) of the PCM was reduced accordingly;
- for each of the cases 1–5 of Table 1, calculations were performed for four temperature differences between the base and mean melting temperature of the PCM, namely 6 °C, 12 °C, 18 °C, and 24 °C. In the simulations, this difference was set at $t = 0$ and kept constant through the entire process.

In the simulations, the initial temperature of the whole system was 20 °C, i.e. the PCM was slightly subcooled. Ambient air above the unit was kept at 27 °C.

Density and dynamic viscosity of the liquid PCM depend on its temperature. The density is expressed as

$$\rho = \frac{\rho_l}{\beta(T - T_l) + 1}, \tag{1}$$

where ρ_l is the density of PCM at the melting temperature T_l, and β is the thermal expansion coefficient. The value of $\beta = 0.001$ has been chosen based on the analysis of the detailed data presented by Humphries and Griggs [7].

Following Reid et al. [31], the dynamic viscosity of the liquid PCM has been expressed as

$$\mu = \exp\left(A + \frac{B}{T}\right), \tag{2}$$

where $A = -4.25$ and $B = 1790$ are coefficients. The properties of the PCM are summarized in Table 3.

2.2. Computational procedure

A three-dimensional computational domain was defined, as shown in Fig. 1b and c, by the symmetry planes of the fin and the PCM-filled gap in the horizontal x_1-direction, by the physical boundaries of the unit in the vertical x_2-direction, and by the included conducting end walls in the horizontal x_3-direction. The origin of the coordinate system was taken at the intersection of the plane of symmetry of the fin and the lower boundary of the fin and PCM.

The numerical approach made it possible to calculate the processes that occur inside the fins and end walls (solid), PCM (solid/liquid), and air (fluid) simultaneously, and to account for the moving boundary due to the variation of the PCM volume. A heat-conduction problem has been solved for the fins and the end walls. The conservation equations for air were solved only in the small domain bounded by the fin on the left, symmetry plane on the right, PCM from below and the plane connecting the fin tips from above. Laminar flow inside the air and liquid PCM was assumed.

It is worth to note that the PCM in the system considered herein is a sole heat sink which is supposed to accumulate all the heat coming from the hot plate. Accordingly, the role of air is to allow for the PCM volumetric expansion, rather than to remove heat. Forced convection on the outer side of PCM would not help due to the high heat capacity and low thermal conductivity of the PCM.

In order to describe the PCM-air system with a moving internal interface but without interpenetration of the two media,[1] a so-called "volume-of-fluid" (VOF) model has been used. In this model, if the nth fluid's volume fraction in the computational cell is denoted as α_n, then the following three conditions are possible: if $\alpha_n = 0$ the cell is empty of the nth fluid; if $\alpha_n = 1$ the cell is full of the nth fluid; and if $0 < \alpha_n < 1$ the cell contains the interface between the nth fluid and one or more other fluids. Thus, the variables and properties in any given cell are either purely representative of one of the media, or representative of a mixture of the media, depending upon the volume fraction values.

For the phase-change region inside the PCM, enthalpy-porosity approach [32–34] was used, by which the porosity in each cell is set equal to the liquid fraction in that cell. Accordingly, the porosity is zero inside fully solid regions. It is worth to note here that Bertrand et al. [12] present the results of a comparison exercise in which various numerical approaches were applied to a phase-change problem that included coupled natural convection and melting, covering two ranges of Prandtl numbers, which corresponded to the melting of metals and organic materials. The results indicate that enthalpy methods are to be used in most phase-change problems where a solid–liquid interfacial region is present between the phases.

Accordingly, the governing equations used here for the PCM-air system are:

[1] The term "medium" is used here instead of "phase" in order to prevent confusion with the solid and liquid phases of the PCM.

Table 3
Properties of PCM used in the detailed study, cases 1–5

Melting point (°C)	Latent heat (kJ/kg)	Density (liquid state) (kg/m^3)	Thermal conductivity (W/m K)	Specific heat (J/kg K)	Dynamic viscosity (g m/s)
23–25	206	$\frac{750}{0.001(T-296)+1}$	0.15	2500	$\exp\left(-4.25+\frac{1790}{T}\right)$

$$\text{continuity} \quad \frac{\partial \alpha_n}{\partial t} + u_i \frac{\partial \alpha_n}{\partial x_i} = 0 \tag{3}$$

$$\text{momentum} \quad \frac{\partial}{\partial t}(\rho u_i) + \frac{\partial}{\partial x_j}(\rho u_j u_i) = \mu \frac{\partial^2 u_i}{\partial x_j \partial x_j} - \frac{\partial p}{\partial x_i} + \rho g_i + S_i \tag{4}$$

$$\text{energy} \quad \frac{\partial}{\partial t}(\rho \hbar) + \frac{\partial}{\partial x_i}(\rho u_i \hbar) = \frac{\partial}{\partial x_i}\left(k \frac{\partial T}{\partial x_i}\right) \tag{5}$$

where α_n is the nth fluid's volume fraction in the computational cell, ρ is the density, k is the thermal conductivity, μ is the dynamic viscosity, S_i is the momentum source term, u_i is the velocity component, x_i is a Cartesian coordinate, and $\hbar$ is the specific enthalpy. The latter is defined as a sum of the sensible enthalpy, $\hbar_s = \hbar_{\text{ref}} + \int_{T_{\text{ref}}}^{T} c_p \, \mathrm{d}T$, and the enthalpy change due to the phase-change γL, where $\hbar_{\text{ref}}$ is the reference enthalpy at the reference temperature T_{ref}, c_p is the specific heat, L is the specific enthalpy of melting (latent heat of the material), and γ is the liquid fraction during the phase change which occurs over a range of temperatures $T_s < T < T_l$, defined by the following relations:

$$\gamma = 0 \quad \text{if } T < T_s, \quad \gamma = 1 \quad \text{if } T > T_l,$$
$$\gamma = \frac{T - T_s}{T_l - T_s} \quad \text{if } T_s < T < T_l \tag{6}$$

The source term S_i in the momentum equation, Eq. (4), is given by

$$S_i = -A(\gamma) u_i \tag{7}$$

where $A(\gamma)$ is the "porosity function" defined by Brent et al. [33], who maintain that "the basic principle is gradually to reduce the velocities from a finite value in the liquid, to zero in the full solid, over the computational cells that are changing phase". Definition of $A(\gamma)$ makes the momentum equation "mimic" Carman–Kozeny equations for flow in porous media:

$$A(\gamma) = \frac{C(1-\gamma)^2}{\gamma^3 + \varepsilon} \tag{8}$$

where $\varepsilon = 0.001$ is a small computational constant used to avoid division by zero, and C is a constant reflecting the morphology of the melting front. This constant is a large number, usually 10^4–10^7. The value of $C = 10^5$ has been used in the present study. In addition, sensitivity of the results to the value of C has been checked by setting the value of $C = 1.6 \times 10^6$, as used by Brent et al. [33] and Pal and Joshi [23]. The difference in the results was not significant.

The problem was solved for the temperature by iterations involving the energy equation, Eq. (5), and the liquid fraction relation, Eq. (6), using the approach of Voller and Swaminathan [35], in which the phase change rate is linearized as a truncated Taylor series, and old iteration values are then used to estimate the linear term.

The numerical solution has been obtained using the Fluent 6.0 software. The SIMPLE algorithm has been used for pressure-velocity coupling. The computational grid was built of $13 \times 100 \times 80 = 104{,}000$ cells. This number was kept constant, while the size of the system itself varied. The grid size was chosen after careful examination of the results of grid refinement process. The time step in the calculations was as small as 0.01 s, and has been chosen after a careful examination of the preliminary calculations for one variant. Further decrease to 0.005 s did not show any noticeable change in the instantaneous results for the heat flux and melt fraction through the whole process, i.e. from $t = 0$ to the complete melting of the PCM. The convergence was checked at each time step, with the convergence criterion of 10^{-5} for the velocity components in x_1-, x_2- and x_3-directions and continuity, and criterion of 10^{-8} for energy.

Two different computers were used for the simulations. We started with a Pentium 4 computer (CPU 1500 MHz, 512Mb RAM). However, it typically took as much as five hours of calculations to simulate one second of physical time. Then, the authors were given access to a Dell PowerEdge 2600 computer, which features two 3.20 GHz Intel Xeon processors and is scalable to 12Gb of PC2100 DDR SDRAM. That computer made it possible to reduce the calculation time to about 30 minutes per physical second, i.e. 10-fold. Still, it could be expected that the planned research program would extend to a very large period of time. For this reason, two-dimensional simulations were considered, as discussed below.

3. Results and discussion

In this section, we present first a comparison of the results obtained in three- and two-dimensional simulations. Then, the results of the parametric study are discussed and analyzed. The discussion concerns the

calculated heat fluxes and melt fractions of the PCM as functions of time. Then, dimensional analysis is used to show the trends and relations, which may lead to generalization of the results.

3.1. Results

The numerical simulations in our study were conducted in a three-dimensional system of non-adiabatic walls, testing the applicability of two-dimensional simulations to a real system.

Fig. 2a–c shows an example of the three-dimensional results for case 2 of Table 1, with the third dimension of the system equal to $l = 24$ mm, and a temperature difference of $\Delta T = 12$ °C. Fig. 2a shows phase distribution of the PCM in an x_2-x_3 plane of symmetry of the system, introduced in Fig. 1c, for the melt fraction of $V/V_0 = 0.3$. Fig. 2b shows the phase distribution in the same plane for a later stage in the process, $V/V_0 = 0.6$. Fig. 2c shows, for the same stage, the cross-sectional phase distribution of the PCM (plane x_1-x_2). Two cross-sections are shown: one is in the plane of symmetry of the system, and the other is 2 mm from the end-wall. One can see that the phase distribution in these cross-sections is, essentially the same. This result indicates that the melting process is close to be two-dimensional.

Fig. 2d shows, for the same stage of $V/V_0 = 0.6$, the cross-sectional phase distribution of the PCM (plane x_1-x_2) obtained in a two-dimensional simulation. It is obvious that this distribution does not differ from those presented in Fig. 2c. Fig. 2a and b shows, however, that the regions close to the conducting end walls are affected by the heat transfer from the end walls, representing three-dimensional effects that could not be captured by a two-dimensional simulation. In order to estimate these effects, the instantaneous heat fluxes were calculated for the whole melting process. Fig. 3 shows the heat flux as a function of time for three- and two-dimensional simulations of the same case. One can clearly see that the results throughout the whole process of melting practically coincide. As mentioned above, the three-dimensional simulations were time-consuming. The results presented in Figs. 2 and 3 were typical for the system in question, and made it possible to proceed with the two-dimensional simulations only.

Dependence of the heat fluxes and melt fractions on the geometrical and thermal parameters of the system is illustrated in Fig. 4. Since it has been found that the behavior of the system is similar for various cases and temperature differences, only representative examples are shown in this figure. Full results will be presented in a dimensionless form in Section 3.2.

Fig. 4a and b represent the calculated mean heat flux, q'', and the volumetric melt fraction, respectively, as a function of time, for case 3 of Table 1. The curves are displayed for $\Delta T = 6$ °C, 12 °C, 18 °C, and 24 °C. As

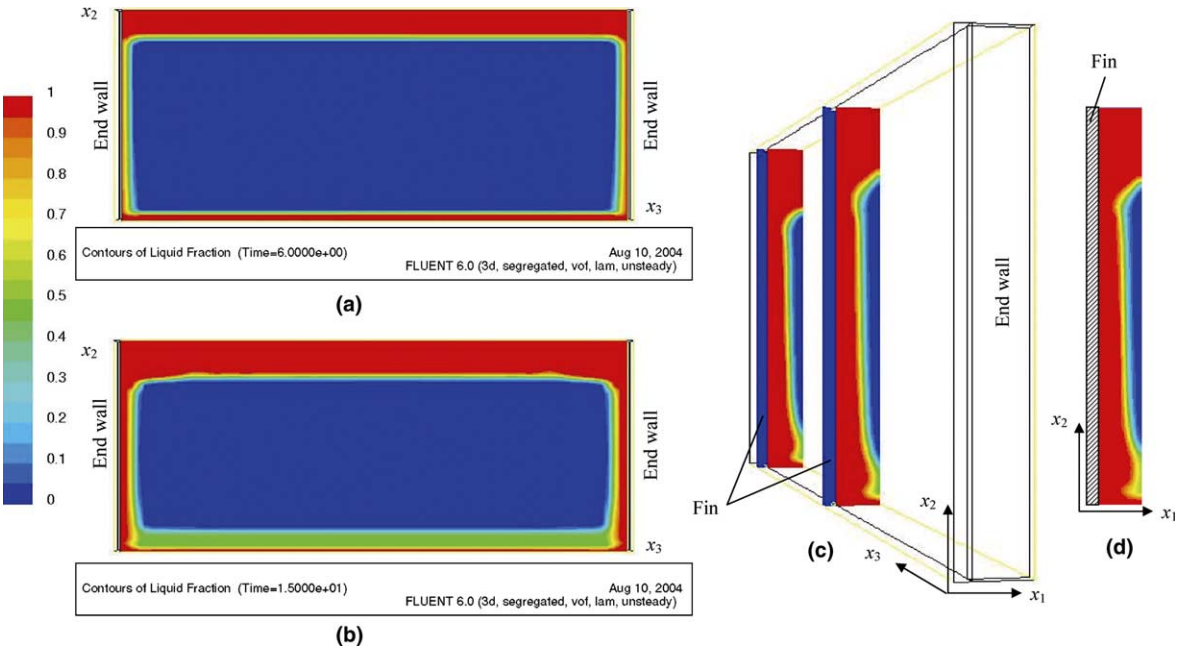

Fig. 2. Examples of three- and two-dimensional simulations (case 2, $\Delta T = 12$ °C): (a) three-dimensional simulation, melt fraction of 0.3, x_2–x_3 plane; (b) three-dimensional simulation, melt fraction of 0.6, x_2–x_3 plane; (c) three-dimensional simulation, melt fraction of 0.6, x_1–x_2 plane; and (d) two-dimensional simulation, melt fraction of 0.6, x_1–x_2 plane.

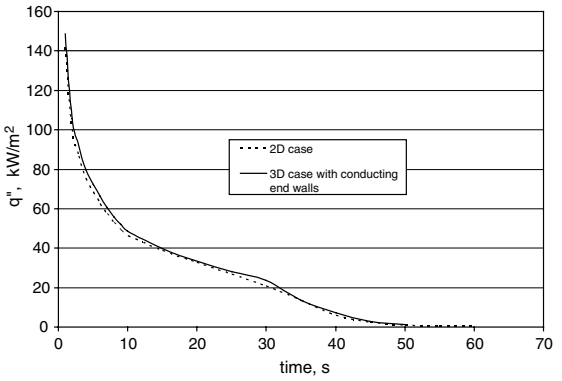

Fig. 3. Comparison of three- and two-dimensional simulations (case 2, $\Delta T = 12$ °C), in terms of heat flux as a function of time throughout the melting process.

expected, the heat flux transferred to the PCM is maximal at the beginning and approaches the natural convection limit when the melting is complete. The larger is the temperature difference, ΔT, the higher is the heat flux initially, and the shorter is the melting time. Consequently, the larger is the ΔT, the steeper is the decrease in heat flux. The same applies to the melt fraction: the higher the base temperature the more rapid is the growth of the melt fraction.

Fig. 4c represents the calculated mean heat flux, q'', as a function of time, for cases 1–5 of Table 1 at $\Delta T = 18$ °C. One can see from the figure that as the width of the system decreases while its height is preserved, cases 1–4, the heat flux increases at the early stages of the process. For the "short" system, case 5, the heat flux is lower.

The total heat flux from the base can be subdivided to the flux transferred into the PCM directly from the base, and the flux transferred into the PCM through the fins. As shown by Shatikian et al. [30], in the large system heat was transferred to the PCM mostly through the conducting partitions, while the heat transfer directly from the heated base was less significant. For a small system considered here, the results are similar, but not identical for the systems of different thicknesses: when the PCM layer between the fins is thick, the fraction of the total heat which is transferred from the base directly to the PCM increases.

Fig. 4d presents the calculated volumetric melt fraction as a function of time, for the cases 1–5 and the same temperature difference as shown in Fig. 4c. One can see from the figure that as the width of the system decreases, while its height is preserved, cases 1–4, the melt fraction grows more rapidly with time. For the "short" system, case 5, this growth is more rapid than for the "high" system of the same width, case 2.

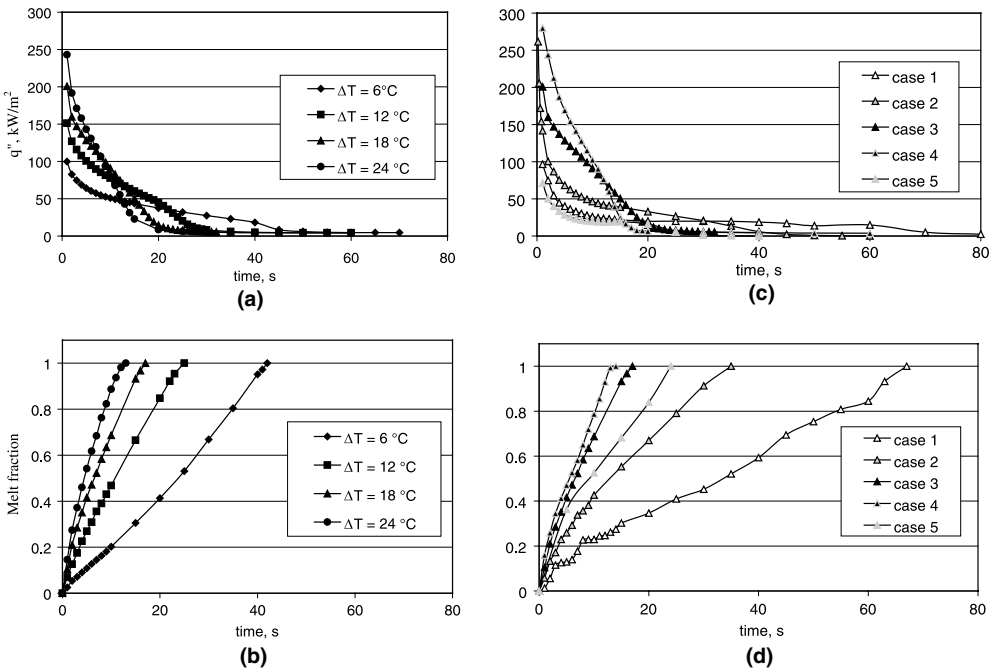

Fig. 4. Examples of the results for heat flux and melt fraction: (a) heat flux for case 3; (b) melt fraction for case 3; (c) heat flux for $\Delta T = 18$ °C; and (d) melt fraction for $\Delta T = 18$ °C.

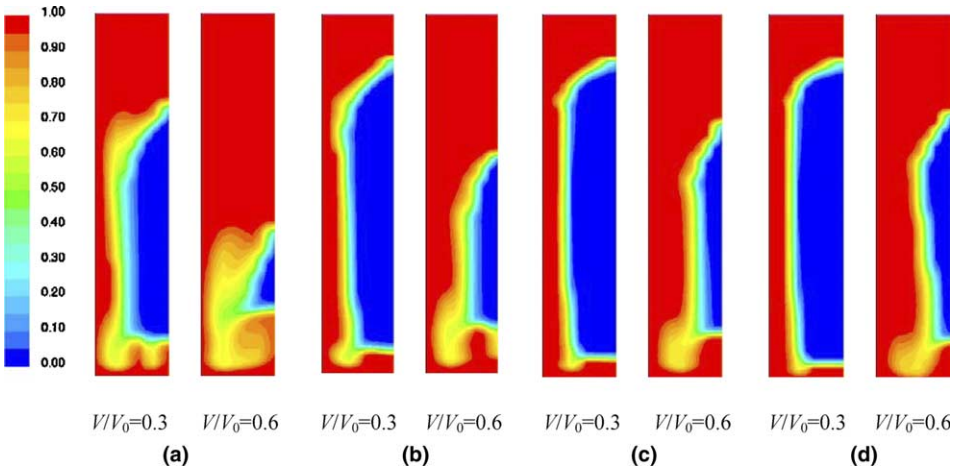

Fig. 5. Evolution of the melting process of the PCM for case 1: (a) $\Delta T = 24$ °C; (b) $\Delta T = 18$ °C; (c) $\Delta T = 12$ °C; and (d) $\Delta T = 6$ °C.

The notation of Fig. 4 is adopted for all the graphs which appear later in the paper, making the results easy to follow.

In order to illustrate the differences in the melting process for different geometries and base temperatures, solid–liquid phase distributions are shown in detail for cases 1–5 in Figs. 5–9, respectively. Each figure shows the phase distributions at the instances which correspond to melt fractions of 0.3 and 0.6, for the temperature differences of (a) 24 °C, (b) 18 °C, (c) 12 °C, and (d) 6 °C. The color scale shows the melt fraction of PCM, V/V_0 from 0 to 1.[2]

One can see from Figs. 5, 6, and 9 that for the "wide" cases the melting front moves generally parallel to the vertical fin. As the width decreases, Figs. 7 and 8, the phase distribution becomes similar to that observed in the preliminary study by Shatikian et al. [30], where a wedge-like solid phase is at the top and the liquid is at the base. In other words, for the "thick" fins melting is almost uniform along the fin surface, while for the "thin" ones melting takes place mostly close to the base. These differences indicate that the temperature distribution in thick and thin fins is different, as discussed below.

3.2. Dimensional analysis

The results discussed above show that the melting process depends on the geometrical and thermal parameters of the system in question. Dimensional analysis is applied now in search of generalized results.

Following a common approach to transient heat conduction problems, we define the dimensionless Fourier number as $Fo = \alpha t/l^2$ where α is the thermal diffusivity of the PCM. A half-thickness of the PCM layer, $l_b/2$, is chosen as the characteristic length. In the present study Fourier number varies from 0 to about 2.6 in case 1 and to about 47.4 in case 4.

The results indicate, however, that the Fourier number alone is not sufficient for generalization even within the same geometrical case. This is because it cannot take into account the phase-change processes. For this reason, the Stefan number should be involved in the analysis, too. It is defined in our case as $Ste = c_p\Delta T/L$, where c_p is the specific sensible heat of the PCM, ΔT is the difference between the heated base temperature and the PCM mean melting temperature, and L is the specific heat of melting. In the present study Stefan number varies from about 0.07 to 0.29.

The product of the Fourier and Stefan numbers, *FoSte*, serves as an independent dimensionless parameter that takes into account the transient heat conduction and phase change. We do not use here the expressions from the literature, like that of Ho and Viskanta [19], because they were derived for an enclosure heated from a side only.

Two dependent dimensionless parameters are used: the melt fraction of the PCM, defined above as V/V_0 and the Nusselt number, which is defined as

$$Nu = \frac{q''}{\Delta T}\cdot\frac{(l_b/2)}{k_{PCM}} \tag{9}$$

i.e. it is based on the mean heat flux, q'', the temperature difference between the base and the PCM mean melting

[2] The software graphics makes a distinction between the "solid" and the "fluid". Hence, the liquid PCM and air are shown by the same color and the PCM-air interface does not appear in the figures. Its level rises constantly during the melting, as shown in a previous study by Shatikian et al. [30].

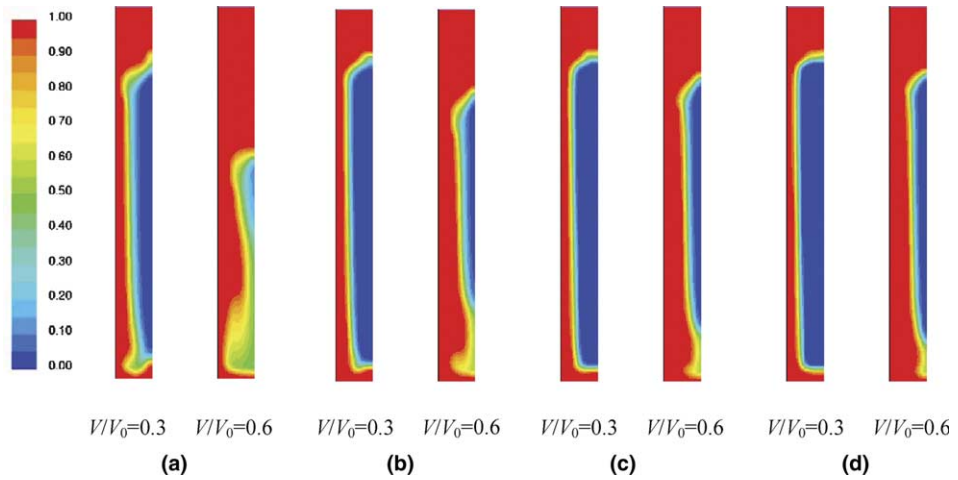

Fig. 6. Evolution of the melting process of the PCM for case 2: (a) $\Delta T = 24$ °C; (b) $\Delta T = 18$ °C; (c) $\Delta T = 12$ °C; and (d) $\Delta T = 6$ °C.

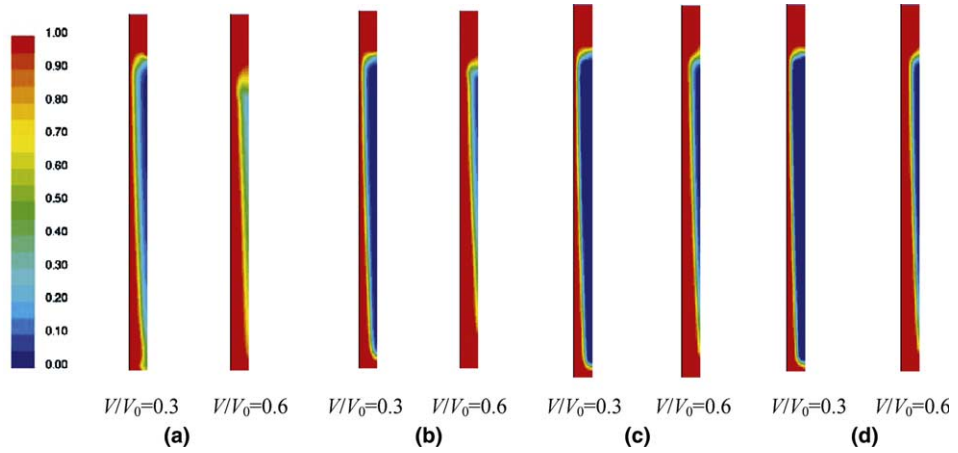

Fig. 7. Evolution of the melting process of the PCM for case 3: (a) $\Delta T = 24$ °C; (b) $\Delta T = 18$ °C; (c) $\Delta T = 12$ °C; and (d) $\Delta T = 6$ °C.

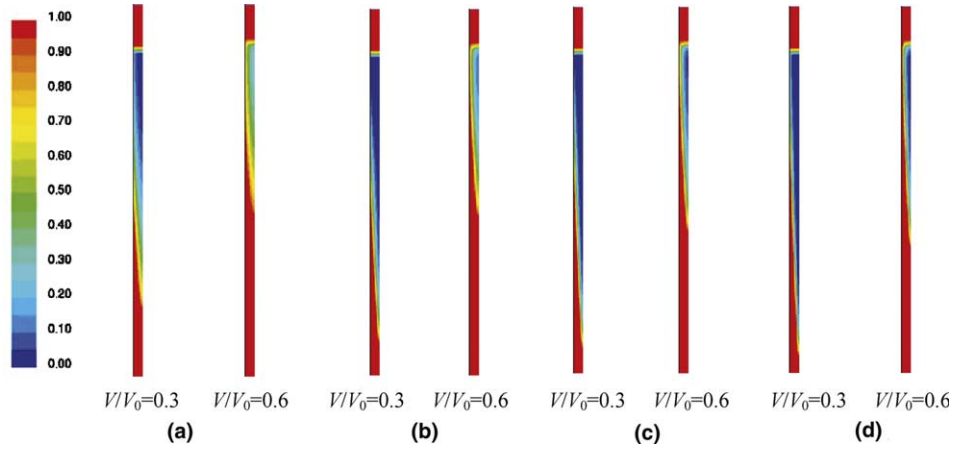

Fig. 8. Evolution of the melting process of the PCM for case 4: (a) $\Delta T = 24$ °C; (b) $\Delta T = 18$ °C; (c) $\Delta T = 12$ °C; and (d) $\Delta T = 6$ °C.

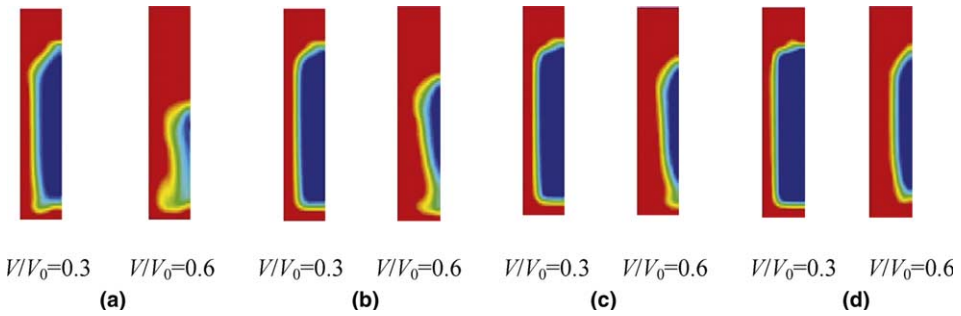

Fig. 9. Evolution of the melting process of the PCM for case 5: (a) $\Delta T = 24$ °C; (b) $\Delta T = 18$ °C; (c) $\Delta T = 12$ °C; and (d) $\Delta T = 6$ °C.

temperature, ΔT, half-thickness of the PCM layer, $l_b/2$, and the thermal conductivity of the PCM, k_{PCM}.

Fig. 10 shows the results for all simulated cases and temperature conditions in a dimensionless form. Fig. 10a,c,e,g,i (upper row) present the Nusselt number for each case, and Fig. 10b,d,f,h,j (lower row) present the corresponding melt fraction.

One can see from Fig. 10 that for both the Nusselt number and the melt fraction in each case, the curves at different ΔT merge into a single curve when the melt fraction is relatively low, up to about 0.4–0.6. At the higher melt fractions, the behavior is different for the "wide" and "narrow" cases: for cases 1, 2, and 5 (Fig. 10b,d,j) the curves diverge at higher melt fractions, while for cases 3 and 4 the curves continue to follow the same pattern. This result is due to the differences in the melting processes for wide and narrow systems, as already discussed in connection with Figs. 5–9. Further analysis of this phenomenon is conducted later in the paper.

One can see from Fig. 10 that for each separate case the behavior of the dimensionless heat fluxes corresponds to the behavior of the melt fractions. When the melt fraction reaches unity, there still is a non-zero (albeit very small) heat flux to the liquid phase, which is cooler than the base.

Fig. 11a–d shows four graphs, each one for cases 1–5, in which the melt fractions are presented vs. *FoSte* for the temperature differences of $\Delta T = 6$ °C (a), $\Delta T = 12$ °C (b), $\Delta T = 18$ °C (c), and $\Delta T = 24$ °C (d) separately. One can see that the results for different cases differ significantly at any given ΔT. This means that the product *FoSte* cannot account for the differences in geometry.

One of the ways to relate to the geometry is to consider the effect of the fin efficiency. Thus, the fin efficiency, η_f, is defined in the literature as the ratio of the actual heat transfer to the heat transfer, were the whole fin at the temperature of the base. It is important to note, however, that the fin efficiency is commonly used to characterize fin performance in a given environment, while in our case the environment is changing throughout the process. Thus, it would not be possible to exactly define the fin efficiency in this case. On the other hand, the considerations related to fin efficiency are still helpful, as shown in the following scale analysis and its outcome in Fig. 11e–h.

The fin efficiency depends on the parameter $l_f\sqrt{hP/k_fA_c}$, which includes the fin length l_f, fin cross-section area A_c, perimeter of this area P, thermal conductivity of the fin material k_f, and the heat transfer coefficient h, from the fin to the surroundings. Some of these parameters are easy to define. For example, in our study, the fin material is the same in all cases, therefore k_f remains constant. For the adopted fin shape, we have $P/A_c = 2/l_t$ where l_t is the fin thickness. We also know the fin length, l_f.

The heat transfer coefficient h, however, varies with the melt fraction. The dependence of h on the process itself makes it impossible to calculate it from the given parameters, which is essential for dimensional analysis.

In order to overcome this difficulty, a scaling procedure is used to estimate the order of magnitude of the heat transfer coefficient. Using the available parameters, we can scale it as $h \sim k_{PCM}/(l_b/2)$, using the thermal conductivity of the PCM and the half-thickness of the PCM layer. This scale analysis provides an insight into the effect of fin parameters on the system behavior, since it is possible now to establish that

$$l_f\sqrt{hP/k_fA_c} \sim \frac{l_f}{l_t}\sqrt{\frac{k_{PCM}}{k_f}}\frac{l_t}{l_b} \tag{10}$$

i.e. the fin efficiency would depend on the ratio of the fin length to its thickness, l_f/l_t. It is worth to note that while the term $(k_{PCM}/k_f)^{1/2}(l_t/l_b)^{1/2}$ in Eq. (10) is constant under the conditions of the present study, it would be applicable also in a more general analysis allowing to include variation in properties and different fin-to-PCM thickness ratios.

We can express now the fin efficiency in the form of $\exp(-C^*l_f/l_t)$, where the efficiency increases with the fin width, decreases with the fin length, and tends to unity when the length approaches zero. C^* is a parameter proportional to the expression $(k_{PCM}/k_f)^{1/2}(l_t/l_b)^{1/2}$.

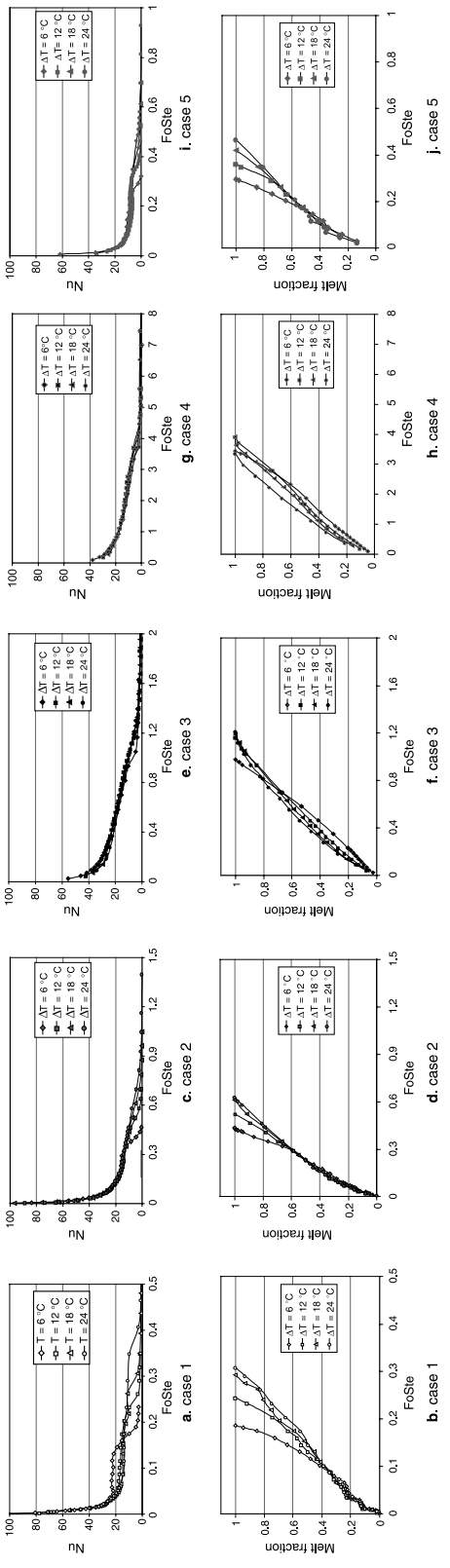

Fig. 10. The Nusselt number and melt fraction vs. the product of *FoSte*: (a,c,e,g,i) Nusselt numbers for cases 1–5, respectively; (b,d,f,h,j) melt fractions for cases 1–5, respectively.

Fig. 11e–h shows four graphs, each one for cases 1–5, in which the melt fractions are presented vs. ($FoSte\exp(-C^*l_f/l_t)$), for the temperature differences of ΔT = 6 °C (e), ΔT = 12 °C (f), ΔT = 18 °C (g), and ΔT = 24 °C (h), corresponding to the four graphs of Fig. 11a–d. The results are shown for C^* = 0.043, which is of the same order of magnitude as the square root expression on the right-hand side of Eq. (10). One can see that now the differences between different cases are much smaller, for all the temperature differences explored in the present study. These results indicate that, although full convergence of different cases has not been achieved, the use of the fin parameters in the analysis is appropriate.

The effect of the transient behavior of the fins is closely related to the PCM melting process. An appropriate choice and definition of the transient parameters could contribute toward a generalized correlation of the PCM melting process in a finned or partitioned system.

Presently we can display the simulated results and analyze the transient performance of the fins. Fig. 12a and b shows the temperature distribution in the fins, of the five cases studied (Table 1) at a temperature difference of 24 °C, and at melt fractions of 0.5 and 0.9, respectively. The temperature is expressed in its dimensionless form, as $(T-T_m)/(T_w - T_m)$, where T_m is the mean melting temperature of the PCM, and T_w is the base temperature. The independent variable is the dimensionless distance from the base, x_2/l_f.

The temperature distribution in the fins clearly shows, that the transient mode dominates all fins throughout the entire process of PCM melting. "Thick" fins, which have the same length to thickness ratio, l_f/l_t, cases 1 and 5, perform at an almost steady state. Namely, their temperature is close to base temperature and almost uniform. The thinner is the fin, the larger is its temperature distribution, as presented for cases 2, 3, and 4 in Fig. 12a and b.

Obviously, the fin temperature distribution affects the melting process, and a relevant parameter related to the fin transient performance has to be chosen. The fin Fourier number is an appropriate parameter, and it has to be defined for the fin length, as the temperature gradient in the one-dimensional fin is longitudinal. By this definition, the same Fourier number represents in our study four out of five cases simulated. Thus, if introduced into the independent variables of Fig. 11, the fin Fourier number could not affect the shape of the curves. However, at this stage, the fin Fourier number may be used in an indicative way to display the approach of the fin to its steady state. This process is illustrated in Fig. 12c, where the temperature of the fin tip is a dimensionless dependent variable. It is shown for cases 1–5 vs. the fin Fourier number.

The figure provides an insight into the phenomena, which were earlier analyzed in Figs. 5–9. There, the

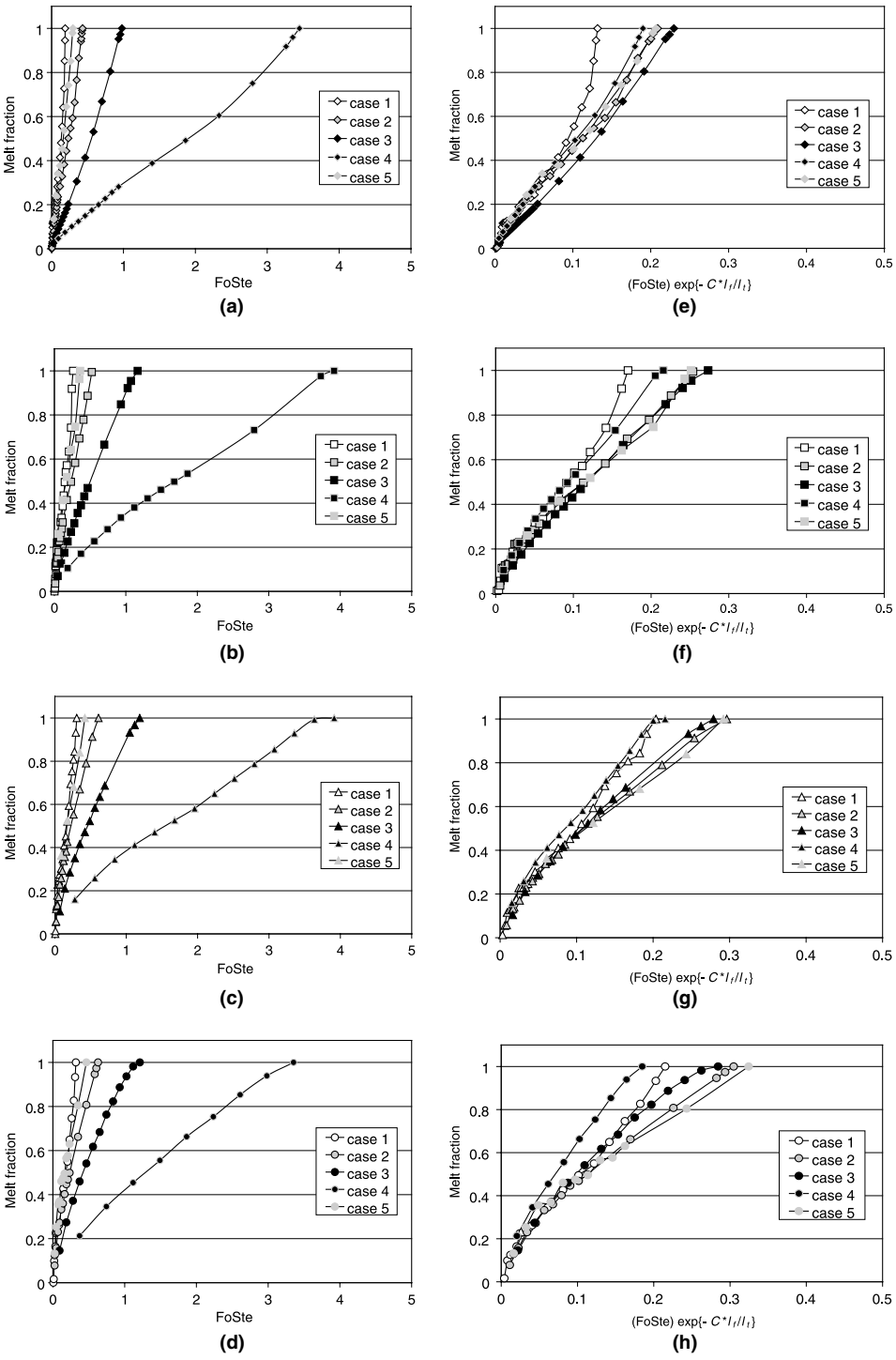

Fig. 11. Melt fractions for each ΔT of the five cases: (a–d) vs. the product of Fourier and Stefan numbers; (e–h) vs. the product of *FoSte* and fin efficiency parameter.

melting process varied with the PCM layer thickness, l_b, which is, of course, related to the fin thickness, l_t, being l_b/l_t = const in our study. Fig. 12c shows us again that the fins of cases 1 and 5 operate at an almost steady state. On the other hand, the thinnest fins, cases 3–4, steeply reach the base temperature after the PCM melt-

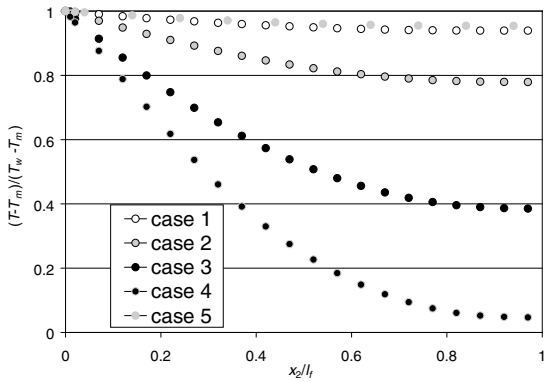

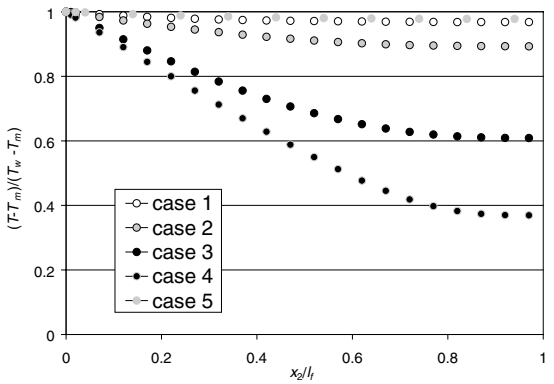

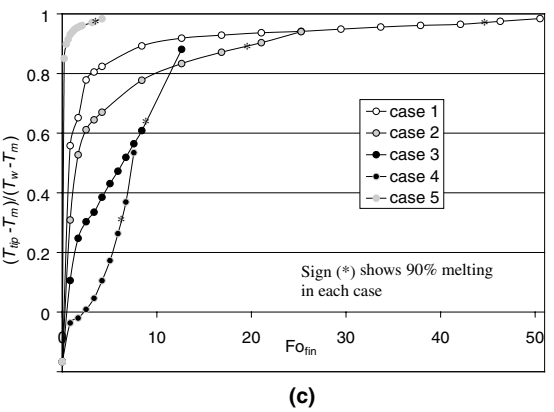

Fig. 12. Dimensionless fin temperature for all cases at $\Delta T = 24$ °C: (a) dimensionless temperature distribution inside the fins for a melt fraction of 0.5; (b) dimensionless temperature distribution inside the fins for a melt fraction of 0.9; and (c) dimensionless temperature of the fin tip as a function of the fin Fourier number.

ing process has been completed. Thus, the fin Fourier number, as a sole representative of the fins transient mode, is useful in the display of those complex phenomena. The fin thickness, l_t, or the length to thickness ratio, l_f/l_t, are dominant geometrical parameters in the transient process, and have been included in the independent variables of Fig. 11e–h.

Until now, we have not discussed a possible effect of the fluid motion on the melting process. Our numerical results indicate that convection in the liquid PCM depends not only on the given geometrical parameters, but also on the melt fraction at a certain time instant. This point is illustrated in Fig. 13, where the vector flow field inside the PCM is shown for the following physical situations: case 1 at melt fractions of 0.3 (Fig. 13a) and 0.6 (Fig. 13b), corresponding to Fig. 5b ($\Delta T = 18$ °C), and case 3 at melt fraction of 0.6 (Fig. 13c), corresponding to Fig. 7b ($\Delta T = 18$ °C). For the same temperature difference, one can see from Fig. 13a and b that in the wide case 1, the flow is weak at $V/V_0 = 0.3$ but becomes stronger at $V/V_0 = 0.6$, while for the narrow case 3 (Fig. 13c) the flow is insignificant even at $V/V_0 = 0.6$. That has been seen also in Fig. 10, where the curves for various ΔT coincided at low melt fractions for both wide and narrow cases. At higher melt fractions the curves diverged in the wide cases (1, 2, 5) but continued to be close in the narrow ones (3, 4). Comparing the results of Figs. 10 and 13, one can conclude that convection in the liquid phase is an additional physical phenomenon that should

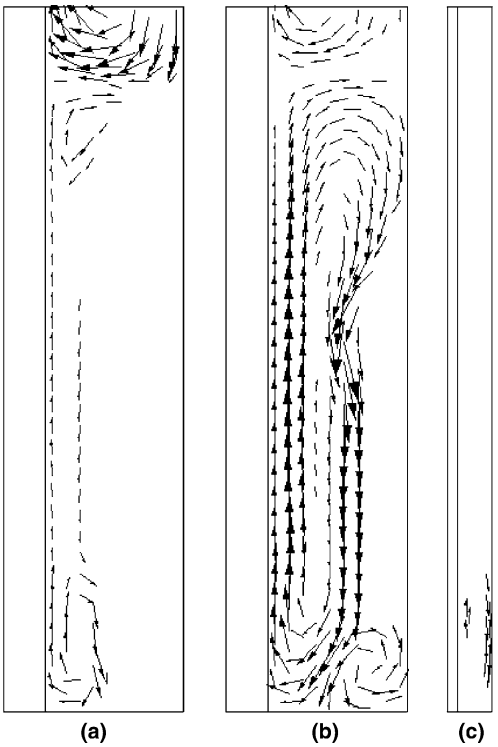

Fig. 13. Simulated velocity fields: (a) case 1 and melt fraction of 0.3; (b) case 1 and melt fraction of 0.6; and (c) case 3 and melt fraction of 0.6.

be accounted for in the analysis for relatively wide layers at high melt fractions.

This could be done using the Rayleigh number. However, it has to be examined whether *Ra* should be based on the height of the PCM layer, as presented by Ho and Viskanta [19], or on its width, resembling the approach common in the analysis of natural convection in enclosures. This problem has been analyzed by Shatikian [36], based on the results summarized by Raithby and Hollands [37] and Gebhart et al. [38]. It has been shown that convective motion in our case is caused by heating from a side, rather than heating from below, which would require unattainable values of the Rayleigh number in the horizontal liquid layer bounded by the fins on its sides and by the solid PCM from above. Accordingly, the characteristic length in the Rayleigh number is based on the height.

Fig. 14 presents the results for case 1, which is the widest of all considered. Fig. 14a reproduces the melt fractions vs. *FoSte* from Fig. 10f, with a significant divergence of the curves for different ΔT. Fig. 14b shows the melt fractions vs. $FoSte/Ra^{1/4}$. The exponent of *Ra* has been chosen based on the laminar natural convection from a vertical isothermal surface, since $Ra \sim O(10^4)$ for the parameters of the present study. One can see from Fig. 14b, that the melt fraction curves for different ΔT almost coincide for the melt fractions of above 0.5. On the other hand, for low melt fractions the curves diverge when plotted vs. a complex containing *Ra*. Similar results are obtained also for the other "wide" cases, namely cases 2 and 5. As for the "narrow" cases 3 and 4, an application of *Ra* leads to divergence of the curves for the whole range $0 < V/V_0 < 1$. Thus, an application of the Rayleigh number should be restricted to "wide" cases, and even there this should be done at high melt fractions only.

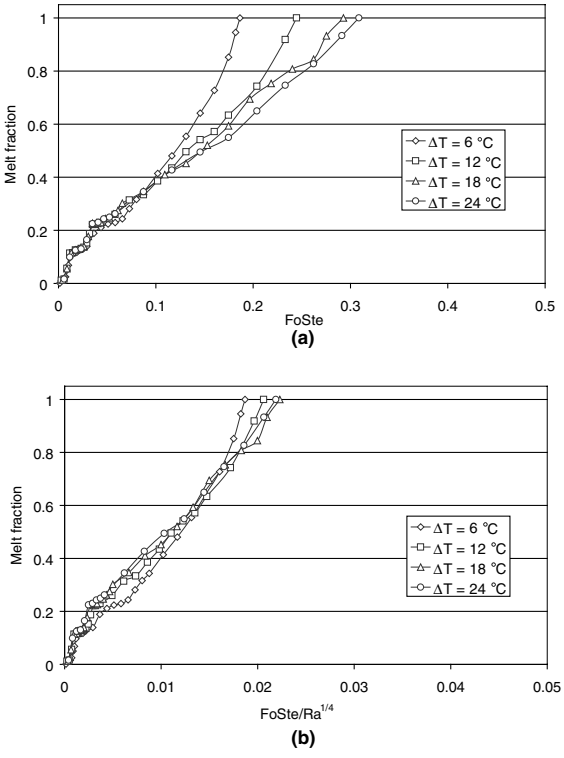

Fig. 14. Melt fractions for case 1: (a) vs. *FoSte*, as in Fig. 10b and (b) vs. $FoSte\ Ra^{1/4}$.

Considering all the different cases, the complexity of the problem, including the multi-dimensionality, non-uniform heating, transient character, irregular melting patterns, and heat transfer to the surroundings, the trends appear similar, in the representation chosen presently.

Some of the findings in the present study will be restricted to the specific geometry of a heat sink with a horizontal base and vertical fins, due to volumetric expansion and gravity effects in the PCM. We have considered here only a constant temperature base, but the trends presented in the dimensional analysis are a step toward generalization.

4. Conclusions

In the present work, the processes of melting of a phase-change material (PCM) in a heat sink with a constant temperature horizontal base, vertical internal fins, and the top open to air, have been studied numerically. Transient two- and three-dimensional simulations were performed using the Fluent 6.0 software. In the simulations, a most complete formulation has been attempted, which takes into account conduction inside the fins, conduction and convection in the PCM, volume change of the PCM associated with phase transition, density and viscosity variation in liquid PCM, and heat transfer to the surrounding air.

In a detailed parametric investigation, the computational results have illustrated how the melting rate, melting front profiles, and heat transfer are affected by the changes in the geometry of the system and the boundary conditions.

Generalization of the results has been attempted through a dimensional analysis. It has been shown that within the same geometry, the Nusselt number and melt fraction depend on the product of the Fourier and Stefan numbers. For relatively wide vertical PCM layers, the Rayleigh number is included, in order to take into account the effect of convection at advanced stages of the melting process. For the different geometrical cases, it has been shown that fin efficiency considerations should be included in the analysis.

The results of the present study broaden the insight into the phenomena of the PCM melting process in a

vertically finned or partitioned system. The simulations illustrate the trends and relations which may lead to generalization, and be used in the design of PCM-based cooling systems.

References

[1] H.E.S Fath, Assessment of solar thermal energy storage technologies, Renew. Energy 14 (1998) 35–40.

[2] A. Kurklu, Energy storage applications in greenhouses by means of phase change materials (PCMs): a review, Renew. Energy 13 (1998) 89–103.

[3] A.G. Evans, M.Y. He, J.W. Hutchinson, M. Shaw, Temperature distribution in advanced power electronics systems and the effect of phase change materials on temperature suppression during power pulses, J. Electron. Packag.—Trans. ASME 123 (2001) 211–217.

[4] S. Krishnan, S.V. Garimella, Thermal management of transient power spikes in electronics–phase change energy storage or copper heat sinks? InterPACK 03: International Electronic Packaging Technical Conference and Exhibition, Maui, Hawaii, July 6–11, 2003.

[5] T.D. Swanson, G.C. Birur, NASA thermal control technologies for robotic spacecraft, Appl. Therm. Eng. 23 (2003) 1055–1065.

[6] D.V. Hale, M.J. Hoover, M.J. O'Neill, Phase-change Materials Handbook, Lockheed Missiles and Space Company, Huntsville, Alabama, 1971.

[7] W.R. Humphries, E.I. Griggs, A design handbook for phase change thermal control and energy storage devices, NASA Technical Paper 1074NASA Scientific and Technical Information Office, 1977.

[8] R. Viskanta, Phase-change heat transfer, in: G.A. Lane (Ed.), Solar Heat Storage: Latent Heat Materials, vol. I, Background and Scientific Principles, 1983 (Chapter 5).

[9] S. Fukusako, M. Yamada, Melting heat transfer inside ducts and over external bodies, Exp.Therm. Fluid Sci. 19 (1999) 93–117.

[10] B. Zalba, J.M. Marin, L.F. Cabeza, H. Mehling, Review on thermal energy storage with phase change: materials, heat transfer analysis and applications, Appl. Therm. Eng. 23 (2003) 251–283.

[11] H. Hu, S.A. Argyroropoulos, Mathematical modeling of solidification and melting: a review, Model. Simul. Mater. Eng. 4 (1996) 371–396.

[12] O. Bertrand, B. Binet, H. Combeau, S. Couturier, Y. Delannoy, D. Gobin, M. Lacroix, P. Le Quéré, M. Médale, J. Mencinger, H. Sadat, G. Vieira, Melting driven by natural convection. A comparison exercise: first results, Int. J. Therm. Sci. 38 (1999) 5–26.

[13] A. Abhat, Low temperature latent heat thermal energy storage: heat storage materials, Solar Energy 30 (1983) 313–332.

[14] R. Velraj, R.V. Seeniraj, B. Hafner, C. Faber, K. Schwarzer, Heat transfer enhancement in a latent heat storage system, Solar Energy 65 (1999) 171–180.

[15] D. Pal, Y.K. Joshi, Application of phase-change materials to thermal control of electronic modules, J. Electron. Packag.—Trans. ASME 119 (1997) 40–50.

[16] K.A.R. Ismail, C.L.F. Alves, M.S. Modesto, Numerical and experimental study on the solidification of PCM around a vertical axially finned isothermal cylinder, Appl. Therm. Eng. 21 (2001) 53–77.

[17] J. Eftekhar, A. Haji-Sheikh, D.Y.S. Lou, Heat transfer enhancement in a paraffin wax thermal storage system, J. Solar Energy Eng. 106 (1984) 299–306.

[18] N.W. Hale Jr., R. Viskanta, Solid–liquid phase-change heat transfer and interface motion in materials cooled or heated from above or below, Int. J. Heat Mass Transfer 23 (1980) 283–292.

[19] C.J. Ho, R. Viskanta, Heat transfer during melting from an isothermal vertical wall, ASME J. Heat Transfer 106 (1984) 12–19.

[20] A. Gadgil, D. Gobin, Analysis of two-dimensional melting in rectangular enclosures in presence of convection, ASME J. Heat Transfer 106 (1984) 20–26.

[21] C. Gau, R. Viskanta, Melting and solidification of a pure metal on vertical wall, ASME J. Heat Transfer 108 (1986) 174–181.

[22] Z. Zhang, A. Bejan, Melting in an enclosure heated at constant rate, Int. J. Heat Mass Transfer 32 (1989) 1063–1076.

[23] D. Pal, Y.K. Joshi, Melting in a side heated tall enclosure by a uniformly dissipating heat source, Int. J. Heat Mass Transfer 44 (2001) 375–387.

[24] G. Casano, S. Piva, Solid–liquid phase change heat transfer: numerical investigation of the wall conduction in the test cell, in: Proceedings of EUROTHERM Seminar 69: Heat and Mass Transfer in Solid–Liquid Phase Change Processes, Bistra Castle, Slovenia, June 25–27, 2003.

[25] H. Inaba, K. Matsuo, A. Horibe, Numerical simulation for fin effect of a rectangular latent heat storage vessel packed with molten salt under heat release process, Heat Mass Transfer 39 (2003) 231–237.

[26] P. Lamberg, K. Siren, Analytical model for melting in a semi-infinite PCM storage with an internal fin, Heat Mass Transfer 39 (2003) 167–176.

[27] P. Lamberg, K. Siren, Approximate analytical model for solidification in a finite PCM storage with internal fins, Appl. Math. Model. 27 (2003) 491–513.

[28] M.J. Huang, P.C. Eames, B. Norton, Thermal regulation of building-integrated photovoltaics using phase change materials, Int. J. Heat Mass Transfer 47 (2004) 2715–2733.

[29] P. Lamberg, R. Lehtiniemi, A.-M. Henell, Numerical and experimental investigation of melting and freezing, processes in phase change material storage, Int. J. Therm. Sci. 43 (2004) 277–287.

[30] V. Shatikian, V. Dubovsky, G. Ziskind, R. Letan, Simulations of PCM melting and solidification in a partitioned storage unit, ASME Summer Heat Transfer Conference, Las Vegas, NV, 2003.

[31] R.C. Reid, J.M. Prausnitz, B.E. Poling, The Properties of Gases and Liquids, McGraw-Hill, New York, 1987, pp. 439–456.

[32] V.R. Voller, M. Cross, N.C. Markatos, An enthalpy method for convection/diffusion phase change, Int. J. Numer. Methods Eng. 24 (1987) 271–284.

[33] A.D. Brent, V.R. Voller, K.J. Reid, Enthalpy-porosity technique for modeling convection–diffusion phase change:

application to the melting of a pure metal, Numer. Heat Transfer 13 (1988) 297–318.
[34] V.R. Voller, An overview of numerical methods for solving phase-change problems, Adv. Numer. Heat Transfer 1 (1996) 341–375 (Chapter 9).
[35] V.R. Voller, C.R. Swaminathan, General source-based method for solidification phase change, Numer. Heat Transfer B 19 (1991) 175.
[36] V. Shatikian, Melting and solidification of a phase-change material with internal fins, M.Sc. Thesis, Heat Transfer Laboratory, Department of Mechanical Engineering Ben-Gurion University of the Negev, approved in May 2004.
[37] G.D. Raithby, K.G. Hollands, Natural convection, in: W.M. Rohsenow, J.P. Hartnett, E.N. Ganić (Eds.), Handbook of Heat Transfer Fundamentals, 2nd ed., McGraw-Hill, 1985 (Chapter 6).
[38] B. Gebhart, Y. Jaluria, R.L. Mahajan, B. Sammakia, Buoyancy-induced Flows and Transport, Hemisphere Publishing Corporation, New York, 1988.